Distribution of In and other rare metals in cassiterite and associated minerals in Sn ± W ore deposits of the western Variscan Belt

Catherine Lerouge, Eric Gloaguen, Guillaume Wille, Laurent Bailly

Eur. J. Mineral.
PrePub DOI: 10.1127/ejm/2017/0029-2673

PrePub Article
Special issue dedicated to Zdeněk Johan

Distribution of In and other rare metals in cassiterite and associated minerals in Sn ± W ore deposits of the western Variscan Belt

CATHERINE LEROUGE[1,*], ERIC GLOAGUEN[1], GUILLAUME WILLE[1,2] and LAURENT BAILLY[1]

[1] BRGM, Water, Environment and Ecotechnologies Division (D3E), 3 Avenue Claude Guillemin, 45060 Orléans, France
*Corresponding author, e-mail: c.lerouge@brgm.fr
[2] ISTO, UMR 7327 - CNRS/Université d'Orléans, 1A rue de la Férollerie, 45071 Orléans Cedex 2, France

Abstract: We present data available on rare metal and indium distributions in cassiterite and associated minerals from thirteen Sn ± W granite-related ore deposits in the western Variscan Belt (Massif Central and Armorican Massif, France; Galicia, Spain; and SW England). Cassiterite and associated minerals including sulfides and titanium oxides were analysed using an electron probe micro-analyzer (EPMA). Significant indium contents were only measured in cassiterite from hydrothermal vein-type mineralizations associated with peraluminous granites of Montbelleux, Abbaretz (French Armorican Massif) and Marcofán (Galicia); they correlate with the highest Nb, Ta and Fe substitutions. Two coupled substitutions are proposed: (1) $2\,(Sn^{4+}, Ti^{4+}) \leftrightarrow (Fe^{3+}, In^{3+}) + (Nb^{5+}, Ta^{5+})$ and (2) $Fe^{2+} + (Nb, Ta)^{5+} \leftrightarrow In^{3+} + (Ti, Sn)^{4+}$ depending on Fe valence state. Sulfides (stannite, chalcopyrite, pyrite, arsenopyrite and sphalerite) and rutile associated with cassiterite contain significant amounts of indium, even when cassiterite is indium-free, suggesting preferential partitioning into the sulfides.

Key-words: cassiterite; tin; indium; tungsten; ore deposit; trace element; sulphides; mineral chemistry.

1. Introduction

The element indium (In) was discovered by Ferdinand Reich and Theodor Richter in 1863 at the Bergakademie Freiberg in polymetallic Ag-base metal ores of the local Freiberg district (Erzgebirge, Germany) with a spectrograph (Seifert & Sandmann, 2006). Indium is a chalcophile element used in industry for its semiconductor and optoelectronic performance. Due to its softness, In alloys can be plated onto metal or evaporated onto glass in a variety of high-tech applications, including screens and monitors, infrared detectors, high-speed transistors, diodes, and photovoltaics. Indium is present as traces in the Earth's crust, but does not form primary ore deposits, and is currently extracted as a by-product of Zn, Sn and Cu deposits (Werner *et al.*, 2017). The growing use of In in high-tech applications and a restricted supply dependent on only a few present-day producers (*e.g.*, China, Korea, Japan, Canada, Zhang *et al.*, 2015) created challenges to In sourcing worldwide (EU Commission, 2014; Werner *et al.*, 2017).

During the two last decades, mineralogical studies of ore deposits in numerous countries have shown that In is a dispersed element present in various deposit types (Schwartz-Schampera & Herzig, 2002; Schwarz-Schampera, 2014; Werner *et al.*, 2017) and usually shared between several mineral phases (*e.g.*, Pavlova *et al.*, 2015; Andersen *et al.*, 2016; Frenzel *et al.*, 2016; George *et al.*, 2016; Werner *et al.*, 2017). Eighteen In minerals are currently identified, among them, roquesite, petrukite, sakuraiite, indite, laforêtite, dzhalindite (Andersen *et al.*, 2016). In many In-rich deposits, the In minerals are not abundant or even absent. The Kawazu Au–Ag–Cu–Mn–Te epithermal ore deposit in Japan is an exception. Roquesite and dzhalindite are its main ores (Shimizu *et al.*, 2008). In other In-rich deposits, the element is instead substituted in a wide variety of minerals, including base-metal sulfides (Fe-rich sphalerite), copper sulfides (chalcopyrite, bornite), copper-tin sulfides (chalcostannate group, stannite), tin oxides (cassiterite) (*e.g.*, Seifert & Sandmann, 2006; Cook *et al.*, 2011a, b, c; Dill *et al.*, 2013; Pavlova *et al.*, 2015; Andersen *et al.*, 2016; George *et al.*, 2016; Frenzel *et al.*, 2016; Valkama *et al.*, 2016); at this time sphalerite represents about 95% of global In production. The major In-rich deposits are, by decreasing order of importance, sediment-hosted massive sulfides, volcanogenic massive sulfides (VMS), skarn, epithermal, and porphyry; sediment-hosted Pb–Zn and VMS represent more than 60% of In resources (Werner *et al.*, 2017). Magmatic-hydrothermal mineralizations mostly associated with post-collisional magmatic pulses, including skarn-, greisen-, and vein-type mineralization, also represent promising exploration targets for In (SE Finland; Erzgebirge/Krušné Hory; Far East Russia; SW England; South China Tin Belt) (Seifert, 2008; Cook *et al.*, 2011c; Pavlova *et al.*, 2015; Seifert *et al.*, 2015; Andersen *et al.*, 2016; Valkama *et al.*, 2016).

DOI: 10.1127/ejm/2017/0029-2673
0935-1221/17/0029-2673 $ 6.75

The Variscan Belt contains several ore deposits identified for their significant In resources (Werner *et al.*, 2017), including VMS in Portugal such as Neves Corvo (Pinto *et al.*, 2014) or Lagoa Salgada (Figueiredo *et al.*, 2012), different ore-deposit types in the Erzgebirge, eastern Germany (skarn-type ores in the Pöhla district: Schuppan & Hiller, 2012; Bauer *et al.*, 2017; Jeske & Seifert, 2017), polymetallic Sn(-Ag)-base metal vein- and greisen-type deposits in the old Freiberg, Marienberg, Annaberg, and Ehrenfriederdorf-Geyer mining districts (Seifert *et al.*, 1992; Jung & Seifert, 1996; Seifert & Sandmann, 2006; Seifert, 2015) and Sn deposits in SW England (Andersen *et al.*, 2016). According to these recent investigations, late-Variscan granite-related Sn mineralizations might also represent potential interesting In targets.

In this work, we present data available on rare-metal and In distribution in cassiterite and associated minerals of Sn ± W ore deposits from Massif Central and Armorican Massif in France, Galicia in Spain and SW England (Table 1; Fig. 1). The role of cassiterite concentrates for the actual world production of In is minor, and the question of whether In can also be hosted in cassiterite remains poorly defined (Pavlova *et al.*, 2015; Andersen *et al.*, 2016). We analysed cassiterite and associated minerals including sulfides and titanium oxides using an electron probe micro-analyzer (EPMA). We paid particular attention to the EPMA analysis method for trace elements in cassiterite related to interferences between Sn and In X-ray emission lines and to a high detection limit described in previous work (Benzaazoua *et al.*, 2003; Pavlova *et al.*, 2015).

Three topics of interest are (1) substitutions of In and other minor and trace elements, such as, Fe, Ti, Nb, Ta and W in the cassiterite lattice, (2) the In distribution among cassiterite and associated minerals, and (3) the trace element content in cassiterite, and more specifically the In content, in terms of ore deposit type.

2. Metallogeny in the Variscan Belt, samples and deposits

The European Variscides, extending from the Iberian Peninsula to Sudetic Mountains, are the result of continental collision between Gondwana and Laurussia. This collision caused the development of a polyphased orogeny, lasting more than 100 Ma from the Early Devonian to the Early Permian, and comprising three major successive stages (*e.g.*, Faure *et al.*, 2009; Maierová *et al.*, 2016) of metallogenesis (Marignac & Cuney, 1999). The first stage of the Variscan orogeny (Early Devonian-Early Carboniferous) corresponds to the closure of Rheic Ocean followed by continental subduction. It is during this stage that sediment-hosted Pb–Zn and VMS were deposited (*e.g.*, Lescuyer *et al.*, 1998; Marignac & Cuney, 1999). The second stage (Mississippian) corresponds to the Variscan continental collision. The third stage of the Variscan Belt (Pennsylvanian to Lower Permian) is a syn- to post-orogenic collapse, marked by normal faults, development of granulite metamorphism of the lower crust and emplacement of granites (*cf.* Williamson *et al.*, 1996; Seifert, 2008; Simons *et al.*, 2016). Most of the magmatic-hydrothermal rare-metal mineralizations and hydrothermal W, Sn, Sn–F(Li) sulfide mineralizations are associated with the emplacement of peraluminous granites and rare-metal granites of this stage (*e.g.*, Marignac & Cuney, 1999; Bouchot *et al.*, 2005).

Samples of cassiterite-bearing ores were selected from twelve Late Variscan and the only Ordovician granite-hosted Sn mineralizations/deposits in the Armorican Massif and Massif Central (France), in Galicia (NW-Spain), and in SW England (Table 1; Fig. 1). In the French Armorican Massif, Sn ± W ore deposits were exploited for Sn (Abbaretz, Saint Renan, La Villeder) and for Sn + W (Montbelleux, Chauris & Marcoux, 1994). The Sn deposits La Villeder and Abbaretz are related to the Variscan leucogranites of the South Armorican zone belonging to the ilmenite serie (Chauris & Marcoux, 1994). Mineralization occurs as quartz – cassiterite ± sulfide veins associated with tourmaline + muscovite + beryl + apatite + albite ± fluorine hydrothermal alteration. At the Sn deposit La Villeder, metre-thick ore veins are hosted by the Lizio leucogranite at its periphery in contact with an Ediacarian metapelitic schist. The density of the ore veins increases toward the contact of the granite with schist. At the Abbaretz Sn deposit, low-angle quartz-veins are associated with the cupola of the Nozay leucogranite in contact with the schist of low metamorphic grade. The Saint Renan Sn deposit is located in the Leon block (Faure *et al.*, 2008), a specific geodynamic domain, where late Hercynian intrusives are polyphased (two-mica potassic granite, locally injected by a leucogranite of probable Permian age). Mineralization occurs as wolframite–quartz veins with minor cassiterite and well-developed meta-granite-greisen ore bodies in the northern part of the Saint Renan Massif (Chauris & Marcoux, 1994). Hydrothermal alteration is essentially represented by tourmalinization and muscovitization. Scheelite (but no cassiterite or wolframite) has been found in the porphyritic granite of the central part and in the fine-grained granite of the southern part. The Montbelleux district is different from the other Sn–W mineralizations by its Ordovician age (Chauris & Marcoux, 1994). Mineralization occurs as quartz–cassiterite–wolframite stockwork in a sodic granite and quartz–wolframite veins in schist near the granite contact (Chauris *et al.*, 1989). The stockwork ore type also contains minor stannite, molybdenite, chalcopyrite, arsenopyrite and sphalerite.

The studied Sn deposits of the French Massif Central are a Cu–Sn–Fe ore deposit (Charrier), W(-Sn) ore deposits (Vaulry, Chataigneraie district) and rare-metal ore deposits disseminated within the rare-metal granites (as defined by Černý *et al.*, 2005) of Beauvoir and Montebras. Charrier is a complex ore deposit (Picot & Pierrot, 1963), which is composed of: (1) Cu orebodies hosted by Devonian metasediments and metavolcanics in contact with micro-granite; the massive sulfide ores consist of chalcopyrite, and bornite with inclusions of roquesite, sphalerite, wittichenite, tennantite–tetrahedrite; and (2) magnetite–cassiterite–lep-

Table 1. Description of the Sn deposits of the Variscan Belt and the Ordovician Sn deposit of Montbelleux, selected for this study.

Deposit	Resource	Sn total (t) prod. + reserves	Ore type and hostrock	Main mineralogy	Age (Ma)	References
French Armorican Massif, France						
Abbaretz	Sn	2800 + 9100	Qtz-Cst vein-type in schists and some in the Nozay granite	Apy, Py, Ccp, Mo	~315 Ma	(1)
La Villeder	Sn	160 + 700	Qtz-Cst vein-type and greisen in the Lizio granite	Sch, Apy, Sp, Ccp, Bmu, Mo	316 ± 6 Ma	(1), (2)
Montbelleux	W–Sn	25 + 4800	Qtz-Wolf vein-type in schist; Qtz-Wolf-Cst stockwork in granite sills and associated greisens	Stn, Mo, Ccp, Apy, Sp	470 ± 10 to 426 ± 15 Ma	(3)
Saint Renan	W–Sn	5000	Qtz-Wolf-Cst vein-type and greisen ore bodies in granite		~321 ± 5 Ma	(1), (4)
French Massif Central, France						
Beauvoir	Rare metals (Sn, Ta, Nb, Be, Li)	2000 + 20 000	Magmatic-hydrothermal dissemination in Beauvoir rare metal granite		317 ± 6 Ma	(5), (6)
Montebras	Rare metals (Sn, Ta, Nb, Be, Li)	300 + 1000	Magmatic-hydrothermal dissemination in Montebras rare metal granite		314 ± 4 Ma	(5), (6)
Charrier	Cu–Fe–Sn	760	Mag-Cst-Lepidomelane orebodies in metabasalt	Rqt, Bn, Ccp, Cst		(8)
Vaulry	Sn–W	50	Qtz-Cst-Wolf vein-type in Blond granite		298 ± 1.2 Ma	(6), (7), (9)
Le Prunet, Chataigneraie	Sn–W		Dissemination in metapelitic schist	Py, Apy		(10)
Entraygues, Chataigneraie	Sn–W		Dissemination in metapelitic schist	Ccp, Sp, Apy, Py		(10)
Galicia, NW Spain						
Marcofan, Beariz district			Vein-type and associated greisens dominantly in granite	Apy, Mo, Py, Ccp, Stn, Sch, Gn, Bmt, Bi.	~320 Ma	(11), (12), (13)
Magros, Beariz district			Vein-type and associated greisens emplaced both in leucogranite and schist	Apy, Mo, Py, Ccp, Stn, Sch, Gn, Bis, Bi	~320 Ma	(11), (12), (13)
Cornwall (England)						
St Agnes	Sn	1000–2000	Vein-type and greisen in topaz peraluminous granite	Apy, Sp, Ccp, Bn		(14)

Q1 References: (1) Chauris & Marcoux (1994); (2) Tartèse *et al.* (2011); (3) Chauris *et al.* (1989); (4) Faure *et al.* (2008); (5) Melleton *et al.* (2015); (6) Cuney *et al.* (2002); (7) Vallance *et al.* (2001); (8) Picot & Pierrot (1963); (9) Harlaux *et al.* (2017); (10) Lerouge *et al.* (2007); (11) Gloaguen *et al.* (2003); (12) Gloaguen (2006); (13) Sizaret *et al.* (2009); (14) Andersen *et al.* (2016). Apy: arsenopyrite; Py: pyrite; Qtz: quartz; Mag: magnetite; Mo: molybdenite; Bn: bornite; Sp: sphalerite; Gn: galena; Cst: cassiterite; Sch: scheelite; Rqt: roquesite; Bmt: bismuthinite; Bi: native bismuth; Stn: stannite; Wolf: wolframite.

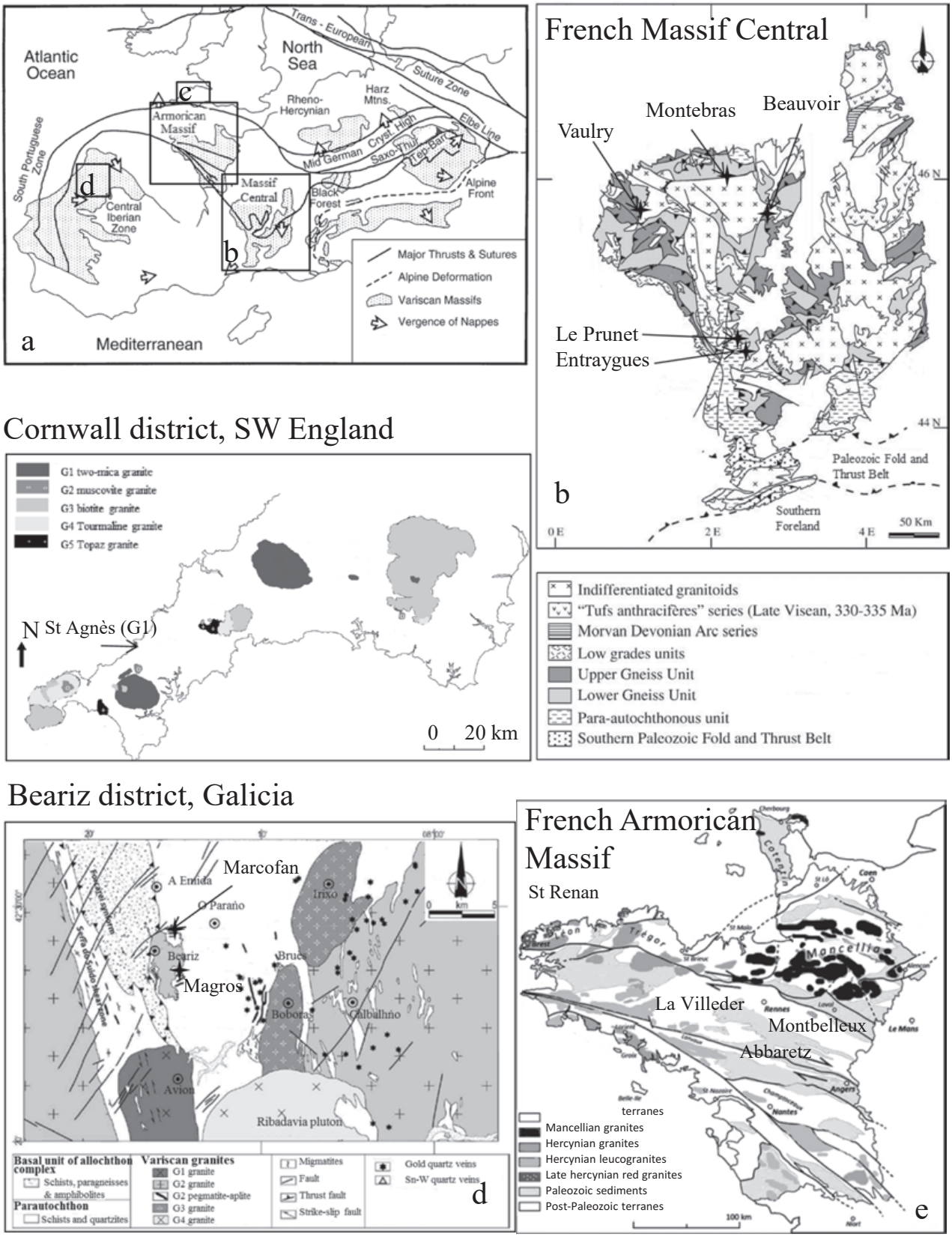

Fig. 1. (a) Schematic map of the Variscan terranes in Europe (after Seifert & Sandmann, 2006); squares indicate the four studied metallogenic provinces. Detailed maps of each province show the distribution of late Hercynian granites and the positions of the studied Sn mineralizations in: (b) French Massif Central (after Melleton *et al.*, 2010), (c) Corwall district in SW England (after Simons *et al.*, 2016), (d) The Beariz district in Galicia, Spain (after Gloaguen *et al.*, 2014) and (e) French Armorican Massif.

idomelane orebodies hosted by metabasalts near the contact with the La Burnolle granite; molybdenite, scheelite, bismuthinite, native bismuth and pyrite are also present.

At Vaulry (northwestern Massif Central), the W–(Sn–Cu) mineralization is hosted by the 310 Ma Li–F-rich Blond rare-metal leucogranite close to its contact with Paleozoic schists (Boulandon, 1989). The Vaulry deposit is characterized by subvertical ore veins, which show three major stages (Vallance *et al.*, 2001): (I) a stage of barren quartz; (II) infill of small fractures by younger quartz, cassiterite and wolframite, and (III) late microcracks infilled with loellingite, chalcopyrite, and pyrite. Stannite, stannoidite, arsenopyrite, bornite with inclusions of roquesite, mawsonite, scheelite, luzonite and molybdenite were also described (Cantinolle *et al.*, 1985; Boulandon, 1989).

The W ± Sn ore deposits of the Chataigneraie district have limited economic potential for W (30 000 t of known WO_3 production distributed across eight deposits; Béziat & Bornuat, 1995), but are not economic for their Sn content. The Sn mineralization is hosted by metamorphic schists in the vicinity of large monzogranites and leucogranitic stocks related to W mineralization at 305 Ma (Lerouge *et al.*, 2000, 2005, 2007). It occurs as late magmatic cassiterite in leucogranite stocks (Entraygues leucogranite) and as hydrothermal cassiterite associated with tourmaline, sulfides and rutile, disseminated in biotite–muscovite–chlorite quartz-rich schist (Le Prunet, Entraygues schist). Typically, sulfides essentially consist of chalcopyrite, sphalerite, arsenopyrite and minor pyrite. The magmatic rare-metal (Sn, Ta, Nb, Be, Li) deposits of Beauvoir and Montebras in northwestern Massif Central are economic (Cuney *et al.*, 1992; Raimbault *et al.*, 1995). The Sn mineralization consists of dominantly disseminated post-magmatic cassiterite associated with a magmatic-hydrothermal paragenesis: lepidolite, topaz, columbo-tantalite, and amblygonite formed at around 570 ± 50 °C (Fouillac & Rossi, 1991). It is hosted by high-phosphorus, peraluminous small albite–lepidolite granitic stocks emplaced between 317 ± 6 Ma for the Beauvoir granite and 314 ± 4 Ma for the Montebras granite (U/Pb columbite-tantalite, Melleton *et al.*, 2015).

The Sn-bearing deposits in central Galicia, NW Spain, are of several types, disseminated within LCT pegmatites or in quartz veins associated with granite intrusions in a district where intrusion-related gold deposits also occur (*e.g.*, Gloaguen *et al.*, 2014). Tin-W ore deposits (Mina Vella mine – Marcofán, Mina Soriana mine – Magros) are located on the eastern side of the late-Variscan Beariz granite (Gloaguen, 2006; Sizaret *et al.*, 2009). Mineralization occurs in N060°E-trending large normal-faulting quartz veins emplaced both in granite and surrounding micaschist. Large hydrothermal alteration zones occur in micaschist as massive tourmalinite haloes closely related to intrusive bodies and quartz veins. Both cassiterite and wolframite occur in the first mineral assemblage that comprises the infill of quartz veins. Marcofán is essentially hosted by granite, whereas Magros consists of veins hosted by schist.

The Saint Agnes Sn–W ore deposit is hosted by a small peraluminous granitic stock associated with the post-Variscan Cornubian Batholith outcropping in SW England (Andersen *et al.*, 2016; Simons *et al.*, 2016). The mineralization consists of quartz–tourmaline–cassiterite–wolframite–chalcopyrite–stannite–sphalerite–löllingite–arsenopyrite veins associated with greisen developed in the apical part of the granitic stock. The greisen alteration minerals include topaz, beryl, apatite and fluorite (Andersen *et al.*, 2016). Textural relationships provide evidence of a high-temperature cassiterite–wolframite ± arsenopyrite–quartz–tourmaline stage followed by arsenopyrite–chalcopyrite with minor stannite stage (Andersen *et al.*, 2016). Roquesite was described in different ore deposits of the Cornwall district (Andersen *et al.*, 2016).

3. Analytical techniques

Images in cathodoluminescence have been acquired on a MIRA 3 XMU (TESCAN, Brno, Czech Republic) equipped with a panchromatic cathodoluminescence detector (350–650 nm) (TESCAN BSE/CL detector) under a low vacuum mode (P = 20 Pa nitrogen).

Analyses of cassiterite and sulfides were performed at the BRGM using a Cameca SX50 EPMA with an accelerating voltage of 20 kV. The spot size was ~1 µm. The system was calibrated with a variety of synthetic oxides and pure elements. Matrix corrections were made with the phi-rho-Z computing program PAP (Pouchou & Pichoir, 1984).

Tin and trace elements in cassiterite were analysed with a beam current of 150 nA. Ti–*K*α, Sn–*L*α, In–*L*α/β, Nb–*L*α were measured on PET, Fe–*K*α on LiF and Ta–*M*α/β, W–*L*α on TAP. Counting times on peak and background were 10 s for Ti and Fe, and 40 s for other elements. Standards of calibration were natural minerals (cassiterite for Sn, roquesite for In), synthetic oxides ($MnTiO_3$ for Ti, Fe_2O_3 for Fe), and pure elements (Nb, Ta and W). Detection of In and Ta in cassiterite is complicated because of interference between the Sn X-ray emission lines and those of In and Ta during EPMA-WDS analyses. The major *L*α line of In (Fig. S1a and b in Supplementary Material, linked to this article and freely available online at the GSW website of the journal: http://eujmin.geoscience world.org) and the major *M*α line of Ta (Fig. S1d) interfere with the positions of the *L*η and the $L\alpha^{2nd\ order}$ lines of Sn, respectively. The contributions of the Sn X-rays to In-*L*α and Ta-*M*α were approximated by analysis of In-free and Ta-free cassiterite and of Sn metal at around 1400 ppm for In and 3000 ppm for Ta. The contribution of the Sn X-ray to the In-*L*α is a value similar to that estimated by Benzaazoua *et al.* (2003). To avoid interference with Sn X-rays, In and Ta were measured on the second major In-*L*β and Ta-*M*β even though their intensities are lower than the intensities of the In-*L*α and Ta-*M*α (Fig. S1c and d). The In-*L*β/In-*L*α intensity ratio is 0.45. The detection limits of the elements are (in ppm): 218 (Ti), 369 (Fe), 238 (Sn), 77 (Sc), 184 (Ta), 144 (Mn), 253 (In), 208 (W) and 313 (Nb).

Elemental mapping of Sn (Sn-$L\alpha$), Ta (Ta-$L\alpha$), Nb (Nb-$L\alpha$), Fe (Fe-$K\alpha$), Ti (Ti-$K\alpha$), and In (In-$L\beta$) in cassiterite were performed on a CAMECA SXFive-FE electron microprobe equipped with a Schottky Field-Emission Gun (FEG) (CAMECA, Gennevilliers – France), using an acceleration voltage of 20 kV and beam current of 200 nA.

Sulfides were analyzed for major and trace elements (S, Cu, Fe, Sn, As, Cd, Zn, In), using a beam current of 20 nA and counting time of 40 s for each element. Standards of calibration were natural minerals (pyrite for Fe, galena for S, sphalerite for Zn, cassiterite for Sn, roquesite for In), synthetic oxides ($MnTiO_3$ for Ti, Fe_2O_3 for Fe), pure elements (Cu) and AsGa (As). The Cd-$L\alpha$, In-$L\alpha$, S-$K\alpha$ and Sn-$L\alpha$ lines were measured on PET, Cu-$K\alpha$, Fe-$K\alpha$, Zn-$K\alpha$ on LiF, and W-$L\alpha$, As-$L\alpha$ on TAP. The detection limits of the elements were (in ppm): 281 (Cu), 178 (Fe), 494 (Sn), 438 (As), 294 (Cd), 293 (Zn), and 306 (In).

4. Ore-mineral composition

4.1. Cassiterite

Cassiterite grains in seventeen samples of the thirteen Sn ore deposits/occurrences were analysed for In and other trace elements. At least 50 analyses were performed in all the cassiterite samples, except for two samples where cassiterite content was very low (Le Prunet, Marcofán6). More analyses were done when In was detected in only small amounts and the amounts of cassiterite allowed it. All data are available in a supplementary electronic file (Table S1) and are presented in summary form with averages and standard deviations in Table 2. Sorting and visual inspection of the data give a good idea of trace element distribution. Averages are low and standard deviations are high compared to averages in most of the cassiterite ores studied because in many analyses, contents were too low to be detected. To provide more representative data, the lowest and highest values, the number of analyses, and the percentage of analyses above the limits of detection are also given. The presence of an element was arbitrarily considered as representative when 20% at least of the analyses were above the limit of the detection. The distribution of Fe, Nb, Ta, Ti and In in cassiterite is highly variable depending on the ore deposit (Fig. 2).

Cassiterite from Saint Agnes is quite pure and only contains traces of Fe and W; it will not be discussed further. Iron is absent or present in small amounts in cassiterite from Beauvoir and Montebras, Magros and Marcofán. Iron is present in significant concentrations in cassiterite from other mineralizations. Considerable concentrations of Nb are present in cassiterite from Abbaretz (1082 ppm), Montbelleux (3901 ppm), Beauvoir (1764 ppm) and Vaulry (590 ppm), and in two samples from Marcofán (#1: 620 ppm; #13: 880 ppm). Tantalum and Ti are both significant trace elements in cassiterite from all the mineralizations, with Ti contents ranging between 326 ppm (Beauvoir) and 4494 ppm (Entraygues) and Ta contents ranging between 393 (Le Prunet) and 5809 ppm (Montbelleux).

Indium is present in cassiterite from Abbaretz, Montbelleux, and two samples of Marcofán (#1, #13): the highest In content is measured in cassiterite of the Ordovician ore deposit of Montbelleux (average: 519 ± 204 ppm, 91% of analyses above the detection limit, max. In content: 1092 ppm). About 20% of the cassiterite analyses of Marcofán (#13, #11) and Abbaretz are above the In detection limit. Indium is absent or systematically lower than the detection limit in cassiterite from Saint Renan, Beauvoir, Entraygues, Le Prunet and Marcofán (#1, #6). Samples from the Sn deposits La Villeder, Charrier, Montebras, Vaulry and Magros had less than 16% of analyses above the detection limit. Cathodoluminescence (CL) and elemental mapping of a cassiterite grain from the Montbelleux Sn–W deposit provide evidence of chemical zoning in Ta, Nb, Ti, Fe and a fine zoning in W, which, however, are not related to the In distribution; the darker zones in CL are richer in Fe (Fig. 3).

4.2. Chemical composition of sulfides

A limited number of EPMA analyses were performed on sulphides that are associated with cassiterite in the thin sections from five Sn ore deposits (Table 3). Chalcopyrite, pyrite and sphalerite in the cassiterite–sulfide dissemination of Entraygues show In contents up to 940 ppm, 930 ppm and 520 ppm respectively. Sphalerite is also characterized by a homogeneous Cd content ~5200 ppm. Chalcopyrite and bornite in the Sn-polymetallic deposit of Charrier show average In contents of ~800 ppm and ~430 ppm, respectively. Chalcopyrite, stannite (Cu_2FeSnS_4) and pyrite from the Marcofán Sn deposit have significant In contents (up to 1220 ppm, 620 ppm and 1540 ppm, respectively), whereas sphalerite shows very low In and high Cd (1.5 wt%) contents. Chalcopyrite (up to 450 ppm), arsenopyrite (up to 640 ppm) and pyrite (up to 740 ppm) from the Magros Sn deposit have lower In contents than sulfides from Marcofán. Chalcopyrite and stannite from the Saint Agnes Sn deposit are characterized by high average In contents of 1560 ppm and 2590 ppm, respectively.

5. Discussion

5.1. Incorporation of trace elements in the cassiterite lattice

For further investigations on major substitutions of trace elements in cassiterite, structural formulae were calculated on the basis of six oxygen atoms. The 1:1 correlation between $3–Sn^{4+}$ and $Fe^{3+} + In^{3+} + Nb^{5+} + Ta^{5+} + Ti^{4+}$ (correlation coefficient r^2 of 0.99) shows that mineral stoichiometry is respected. Tin substitutions by Ti, Fe, Nb and Ta are limited in these cassiterites, the number of Sn atoms varying between 2.88 and 2.99. Binary diagrams of Ti, Fe, Nb and Ta atomic contents reported as a function of (3–Sn) show that all the analyses exhibit the same order of incorporation of trace elements in cassiterite for most of

Table 2. EPMA analyses of cassiterite from the different ore deposits. For each trace element average value, standard deviation and the number of analyses are given. The number of analyses is given to estimate detection limit for a set of data. The detection limits are 369 ppm for Fe, 253 ppm for In, 313 ppm for Nb, 184 ppm for Ta and 218 ppm for Ti.

Ore deposit	Number of analyses		SnO_2	Trace element contents (ppm)				
			wt%	Fe	In	Nb	Ta	Ti
Abbaretz	98	Min	94.20	350	<dl	<dl	<dl	1421
		Max	99.71	3288	419	2517	1998	5419
		Average	98.97	1292	154	1082	444	3006
		Std. dev.		462	122	401	302	770
		% >dl		99	22	90	79	100
Montbelleux	45	Min	95.43	<dl	<dl	<dl	597	647
		Max	99.31	5666	1020	12 282	20 490	5827
		Average	97.83	2568	519	3901	5809	2635
		Std. dev.		1402	204	3487	4325	1377
		% >dl		98	91	84	100	100
La Villeder	50	Min	98.69	<dl	<dl	<dl	753	403
		Max	100.25	1337	379	<dl	1957	8369
		Average	99.70	451	77		1222	3728
		Std. dev.		326	112		200	1471
		% >dl		26	5		50	50
Beauvoir	46	Min	96.61	<dl	<dl	<dl	<dl	<dl
		Max	101.53	979	<dl	5991	3407	1900
		Average	99.96	227		1764	1255	326
		Std. dev.		672		1794	591	537
		% >dl		16		67	90	41
Charrier	57	Min	92.48	630	<dl	<dl	<dl	<dl
		Max	100.10	18 647	597	<dl	1204	24 897
		Average	99.06	3818	109		662	2018
		Std. dev.		4040	139		378	4045
		% >dl		100	16		79	58
Entraygues	124	Min	91.35	<dl	<dl	<dl	<dl	1271
		Max	100.41	22 191	<dl	860	2383	9820
		Average	98.95	1935		120	569	4494
		Std. dev.		2972		191	384	2408
		% >dl		94		5	97	100
Montebras	49	Min	97.77	<dl	<dl	<dl	<dl	468
		Max	100.70	1718	1023	2398	1409	2938
		Average	100.26	186	63	72	1059	1483
		Std. dev.		284	201	356	386	466
				14	6	4	96	100
Le Prunet	21	Min	98.62	<dl	<dl	<dl	188	<dl
		Max	101.21	7788	<dl	<dl	557	10 527
		Average	100.31	1284			393	2355
		Std. dev.		1769			102	2617
		% >dl		52			100	86
Saint Renan	197	Min	98.13	<dl	<dl	<dl	<dl	<dl
		Max	101.28	7718	<dl	2503	1671	11 109
		Average	99.83	658		271	491	2065
		Std. dev.		1365		520	271	2230
		% >dl		30		16	94	82
Vaulry	50	Min	94.51	<dl	<dl	<dl	<dl	<dl
		Max	100.63	7431	617	2181	1499	5198
		Average	99.57	1215	94	590	1185	2787
		Std. dev.		1202	119	703	233	1800
		% >dl		76	8	34	98	74

Table 2. (continued).

Ore deposit	Number of analyses		SnO_2	Trace element contents (ppm)				
			wt%	Fe	In	Nb	Ta	Ti
Magros	50	Min	98.68	<dl	<dl	<dl	401	1007
		Max	99.93	847	425	1601	3456	3741
		Average	99.30	182	78	285	1569	1716
		Std. dev.		196	98	335	908	360
				16	4	16	100	100
Marcofán 1	93	Min	99.78	<dl	<dl	<dl	<dl	1127
		Max	102.09	707	<dl	1202	2293	3327
		Average	100.35	119		620	799	2031
		Std. dev.		134		300	383	571
		% >dl		5		56	99	100
Marcofán 6	11	Min	99.57	<dl	<dl	<dl	7136	1229
		Max	100.65	389	<dl	692	2997	3831
		Average	100.13	228		201	1345	2151
		Std. dev.		114		221	708	1030
		% >dl		9		9	100	100
Marcofán 11	97	Min	99.38	<dl	<dl	<dl	<dl	839
		Max	100.90	583	400	<dl	2310	2578
		Average	100.38	147	148		489	1561
		Std. dev.		144	113		352	435
		% >dl		9	20		94	46
Marcofán 13	52	Min	98.51	<dl	<dl	<dl	532	1709
		Max	99.52	1399	578	2579	7404	3963
		Average	98.98	571	271	880	2913	3100
		Std. dev.		239	134	730	1849	500
		% >dl		83	48	48	100	100

the Sn mineralizations (Fig. S2). The $Sn^{4+} \leftrightarrow Ti^{4+}$ substitution is a major one, which can be considered as the easiest substitution due to the similar properties of Sn and Ti cations and similarity between the rutile [TiO_2] and cassiterite structures. Other Sn^{4+} substitutions by Fe (Fe^{2+} and Fe^{3+}) and rare metals (dominant Ta^{5+} and minor Nb^{5+}) are more complex due to the need to maintain electroneutrality in the crystal. Chemical compositions of cassiterite from different ore occurrences and mining districts are plotted in (Sn, Ti) − (Nb, Ta) − Fe composition diagrams (Fig. 4a–d). Cassiterite from the Sn deposits Beauvoir, Magros and Marcofán, and some cassiterite analyses from the Montbelleux deposit plot along the (Sn, Ti) − (Fe, Mn)$(Nb, Ta)_2$ join, which defines the $Fe^{2+} + 2\ (Nb, Ta)^{5+} \leftrightarrow 3\ (Sn, Ti)^{4+}$ ideal substitution (substitution 1) (Černý *et al.*, 1985; Lerouge *et al.*, 2007). This substitution (1) is also defined in minerals of the tantalite supergroup (Breiter *et al.*, 2005), and micro-inclusions of minerals of the tantalite group have already been observed in cassiterite in Nb–Ta rich systems (Neiva, 2008). That probably implies a limit to Nb, Ta incorporation in cassiterite, which is not well defined to our knowledge. Cassiterite from the Abbaretz Sn deposit and some cassiterite analyses from the Montbelleux Sn deposit plot along the (Sn, Ti) − Fe (Nb, Ta) join, suggesting that incorporation of Fe, Nb, Ta and Ti is rather defined by the $Fe^{3+} + (Nb, Ta)^{5+} \leftrightarrow 2\ (Sn, Ti)^{4+}$ substitution (substitution 2). Analyses of the Fe-rich cassiterites of the Sn deposits Charrier, Saint Renan, and Vaulry that plot along the (Sn, Ti) − (Fe, Mn) join might correspond to a $Fe^{3+} + OH^- \leftrightarrow Sn^{4+} + O^{2-}$ substitution (Möller *et al.*, 1988), but could be due to micrometre-sized inclusions of Fe oxides or ilmenite. Backscattered electron images of cassiterite from these ore deposits did not provide evidence of any inclusions of Fe-bearing phases, favoring the assumption of the substitution.

To conclude, two ideal coupled substitutions (1) $Fe^{2+} + 2\ (Nb, Ta)^{5+} \leftrightarrow 3\ (Sn, Ti)^{4+}$, and (2) $Fe^{3+} + (Nb, Ta)^{5+} \leftrightarrow 2\ (Sn, Ti)^{4+}$ are at least possible for incorporation of Nb and Ta in the cassiterite studied. That has several implications: (1) incorporation will remain low in Fe-poor cassiterite, (2) incorporation will be limited by the formation of tantalite minerals, and (2) incorporation will highly depend on the Fe valence, and consequently on the redox condition in the system.

In regard to In incorporation in cassiterite, homogeneous spot values and mapping of Montbelleux cassiterite indicate that In is in the cassiterite lattice. Assuming that In is present as In^{3+} in the crust (Smith *et al.*, 1978), and that the electroneutrality of the crystal needs to be maintained,

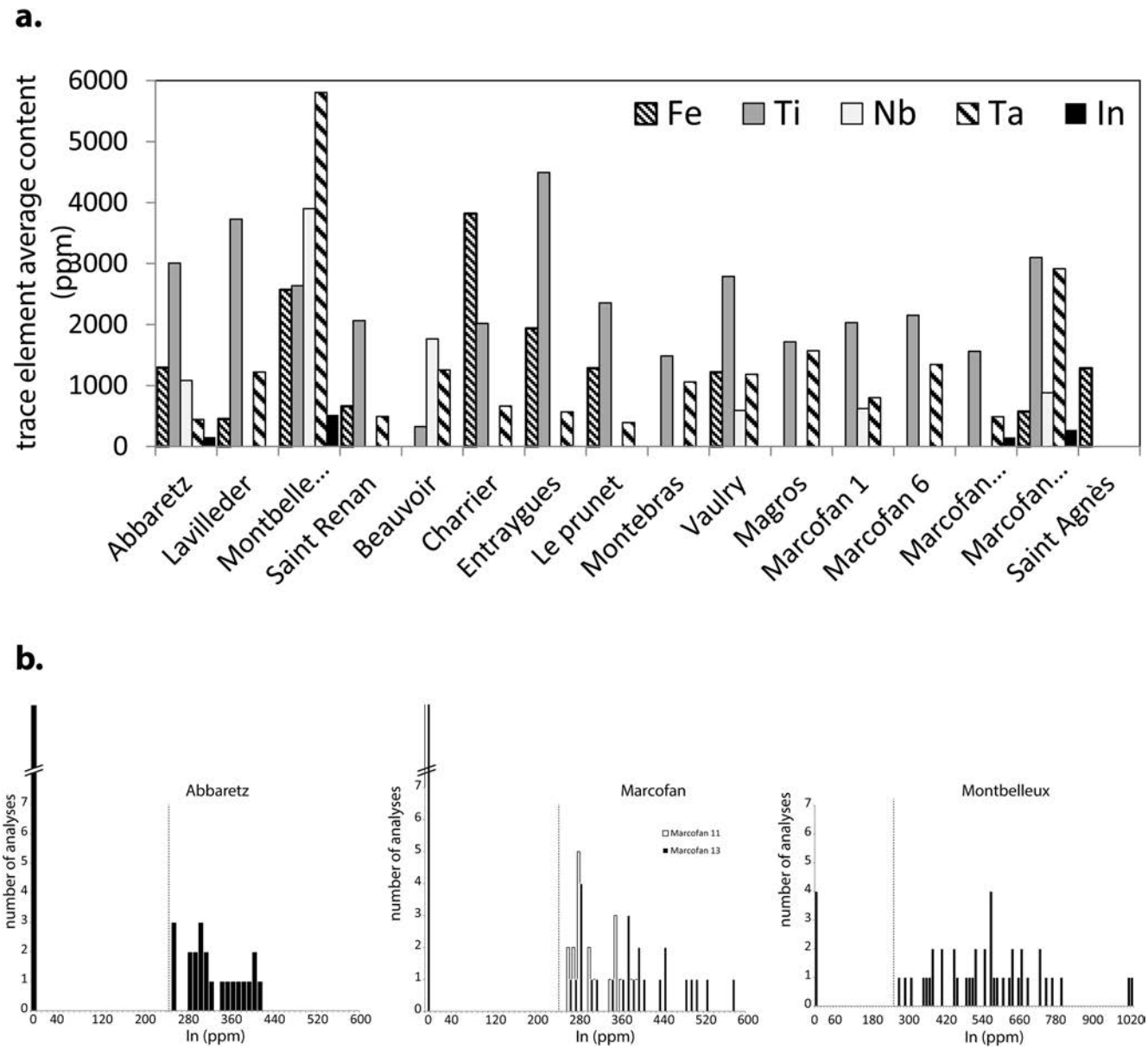

Fig. 2. (a) Histogram showing the average values of Fe, Ti, Nb, Ta and In contents in cassiterite from the thirteen Sn ore deposits; (b) histograms of indium grade distribution (ppm) for some cassiterite from Abbaretz, Marcofán and Montbelleux deposits. Bin size = 10 ppm, EPMA detection limit of 253 ppm is represented by the vertical dotted line on each histogram. The disrupted zero bins represent 78, 78 and 27 analyses for Abbaretz, Marcofán11 and Marcofán13, respectively.

In incorporation may follow the coupled substitution 1: $(Fe, In)^{3+} + (Nb, Ta)^{5+} \leftrightarrow 2\ (Sn, Ti)^{4+}$. Incorporation of In^{3+} in cassiterite via coupled substitution (2) could be possible by modifying the exchange vector as follows: $Fe^{2+} + (Nb, Ta)^{5+} \leftrightarrow In^{3+} + (Ti, Sn)^{4+}$.

5.2. Distribution of In in mineral parageneses

Among the studied deposits, the In mineral roquesite is present at the Sn deposits Charrier, Vaulry and Saint Agnes. In these three deposits, cassiterite shows very low In contents. At the Charrier deposit, the order of In distribution in Zn-poor Cu–Sn ore is discrete roquesite, followed by sphalerite (0.8 wt%), chalcopyrite (800 ppm) and bornite (430 ppm). At Saint Agnes, the In distribution in the studied sample is discrete roquesite followed by stannite (2190 ppm) and chalcopyrite (1565 ppm), in good agreement with Andersen *et al.* (2016).

Cassiterite contains In in only three of the thirteen ore deposits studied: Montbelleux (519 ± 204 ppm), Abbaretz (up to 420 ppm) and Marcofán (up to 580 ppm). Indium contents measured in those cassiterites are consistent with literature data (Briskey, 2005; Pavlova *et al.*, 2015). No sulfides were observed in samples from Montbelleux and Abbaretz. In the Marcofán ore deposit, cassiterite contains In in sulfide-bearing samples (#1: up to 400 ppm, #13: up to 578 ppm); this has already been described by Pavlova *et al.* (2015). The In distribution in

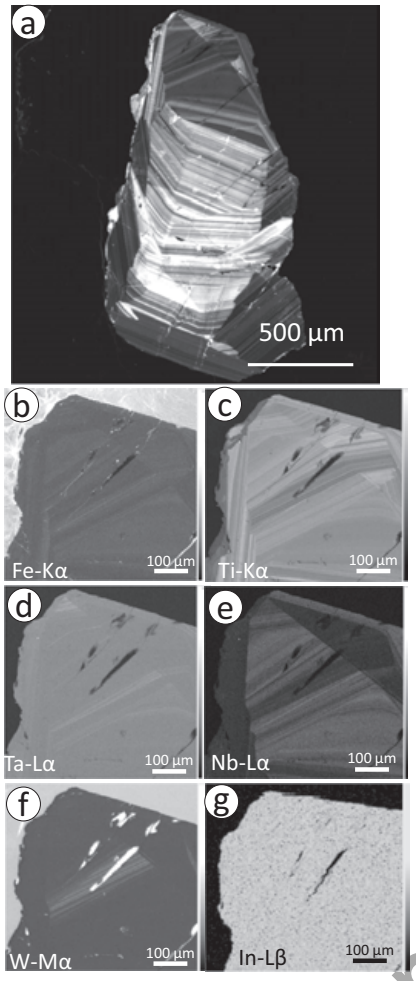

Fig. 3. Mapping of trace elements in cassiterite from the Montbelleux ore deposit. (a) CL image of a single cassiterite grain; (b) to (g) Element mapping of Fe, Ti, Ta, Nb, W and In, using electron microprobe equipped with a Field-Emission Gun (FEG).

Zn-poor Sn–Cu ore of the Marcofán Sn deposit is chalcopyrite (150–730 ppm), followed by cassiterite (150–270 ppm) and stannite (140 ppm).

In other ore samples containing sulfides (Magros and cassiterite–sulfide dissemination of Entraygues), no In mineral is observed and few analyses of cassiterite have detectable In contents, whereas associated sulfides and rutile (when it is analysed) contain In.

The comparative In contents of the different phases from each ore deposit confirm that chalcopyrite, bornite, stannite, pyrite, arsenopyrite, rutile can also contain In. In the studied Sn ore deposits, ores are Zn-poor and Cu-rich, and they are of interest because of the high average In contents in Cu-sulfides: chalcopyrite (up to 2780 ppm); stannite (up to 2670 ppm); bornite (up to 670 ppm).

5.3. Trace element contents in cassiterite and ore deposit type

Mineralizations of the Sn deposits Montebras and Beauvoir consist of magmatic cassiterite disseminated in rare-metal (Sn, Ta, Nb, Be, Li) granites (Černý *et al.*, 2005). Mineralizations of the other Sn deposits of this study are dominantly hydrothermal vein-type (except the mineralizations of Le Prunet and Entraygues schists, which are disseminated in schists) and spatially associated with late Variscan peraluminous granites. These granites result from partial melting of the crust and fractional crystallisation (Cornwall: Simons *et al.*, 2016; French Armorican Massif: Bernard-Griffiths *et al.*, 1985; Chauris & Marcoux, 1994; Tartèse & Boulvais, 2010; Galicia: Gloaguen, 2006; French Massif Central: Williamson *et al.*, 1996). Partial melting was initiated by increased crustal temperature and by F–Li–P fluids derived from granulite metamorphism of the lower crust in relation with processes of underplating of mantle magmas (*cf.* Williamson *et al.*, 1996; Seifert, 2008; Simons *et al.*, 2016).

Even though Sn hydrothermal mineralizations are spatially associated with granites, they are not systematically genetically linked to them (Marignac & Cuney, 1999; Vallance *et al.*, 2001). Case studies of mineralizations provided evidence of a genetic link between mineralizations and peraluminous granites in La Chataigneraie district French Massif Central (Lerouge *et al.*, 2007), in the Beariz district, Galicia (Gloaguen *et al.*, 2014), in Saint Agnes, SW England (Andersen *et al.*, 2016), and in the South Armorican Massif (Chauris & Marcoux, 1994).

In the Sn deposits studied here, two types of cassiterite may be distinguished according to their trace element (Fe, Ti, Nb, Ta) contents. The first population of cassiterite, which is Fe–Ti-rich and Nb–Ta-poor, mostly corresponds to hydrothermal mineralizations hosted by pelitic schists (Entraygues schists, Le Prunet), metabasalts (Charrier) or granite not genetically linked to mineralizations (Vaulry, Vallance *et al.*, 2001). The second population, which is Nb–Ta-rich, corresponds to magmatic mineralizations disseminated in rare-metal granites (Beauvoir and Montebras) and to hydrothermal vein-type mineralisations genetically associated with peraluminous granites and hosted by both granite and pelitic schists (Marcofán and Magros in the Beariz district, Galicia; Abbaretz and LaVilleder, South Armorican Massif; Ordovician Montbelleux). Reported in a binary Fe *vs.* Nb+Ta diagram, analyses of hydrothermal Fe–Ti-rich and Nb–Ta-poor cassiterites plot in the field of hydrothermal cassiterite of Tindle & Breaks (1998) (Fig. 4f). Analyses of magmatic-hydrothermal Nb–Ta-rich cassiterites associated with rare-metal granites (Beauvoir, Montebras) plot in the field of rare-element granites and pegmatites of Tindle & Breaks (1998). On the contrary, analyses of hydrothermal Nb–Ta-rich cassiterites from Montbelleux, Marcofán, Magros, Abbaretz and La Villeder plot in the field of rare-element granites and pegmatites, rather than in the hydrothermal field. Thus the field of rare-element granites and pegmatites defined by Tindle & Breaks (1998) is not so restrictive and would rather correspond to cassiterites that show the coupled substitutions (1) $Fe^{2+} + 2\ (Nb, Ta)^{5+} \leftrightarrow 3\ (Sn, Ti)^{4+}$ and (2) $Fe^{3+} + (Nb, Ta)^{5+} \leftrightarrow 2\ (Sn, Ti)^{4+}$.

It is also noteworthy that the Nb–Ta contents of hydrothermal cassiterites are lower in the Sn deposit La Villeder (granite/schist-hosted) than in the Sn deposit

Table 3. Chemical compositions of sulfides associated with cassiterite in the different studied Variscan Sn ore deposits. The detection limits are 281 ppm for Cu, 494 ppm for Sn, 293 ppm for Zn, 438 ppm for As, and 306 ppm for In.

Deposit	Mineral	Number of analyses	Cu	Fe	Sn	Zn	As	S	Total	Cd (in ppm)				In (in ppm)			
			in wt%							Mean	Std dev	Min	Max	Mean	Std dev	Min	Max
Charrier	Bornite	5	63.30	10.70	<dl	<dl	<dl–0.10	25.84	99.84					434	154	310	670
	Chalcopyrite	9	35.44	28.69	0.06	0.05	<dl–0.09	34.55	98.77					797	263	0	1100
Entraygues	Chalcopyrite	4	34.68	28.93	0.13	<dl	<dl–0.07	34.82	98.55					495	363	0	940
	Pyrite	3	0.06	45.90	<dl	<dl	<dl–0.09	53.69	99.65					540	342	0	930
	Sphalerite	7	0.49	10.80	<dl	53.54	<dl–0.09	33.41	98.24	5266	368	4580	5720	163	188	0	520
Magros	Arsenopyrite	18	<dl	33.74	<dl	0.04	47.21	19.19	100.19	3420	10 685	0	33 830	395	288	0	740
	Chalcopyrite	4	34.01	29.22	0.07	<dl	<dl–0.15	34.41	97.71					154	172	0	450
	Pyrite	2	<dl	46.05	<dl	<dl	<dl–0.84	53.55	99.60					400	349	0	640
Marcofan	Chalcopyrite	16	33.07	29.27	0.06	1.69	<dl–0.018	35.05	99.15			0	2130	727	265	360	1220
	Pyrite	6	<dl	58.18	<dl	1.17	0.08–0.16	39.55	98.90					597	611	0	1540
	Sphalerite	10	<dl	9.40	<dl	55.27	<dl–0.06	33.19	97.86	14 282	563	13 700	14 740				
	Stannite	5	29.30	12.01	27.18	0.74	<dl–0.07	29.70	98.93	326	260	80	720	142	270	0	620
Saint Agnes	Chalcopyrite	8	34.14	26.22	3.71	0.30	<dl–0.05	33.96	98.33	59	120	0	330	1563	594	700	2780
	stannite	7	30.07	11.19	26.39	1.97	<dl–0.04	29.35	98.96	211	198	0	550	2187	372	1790	2670

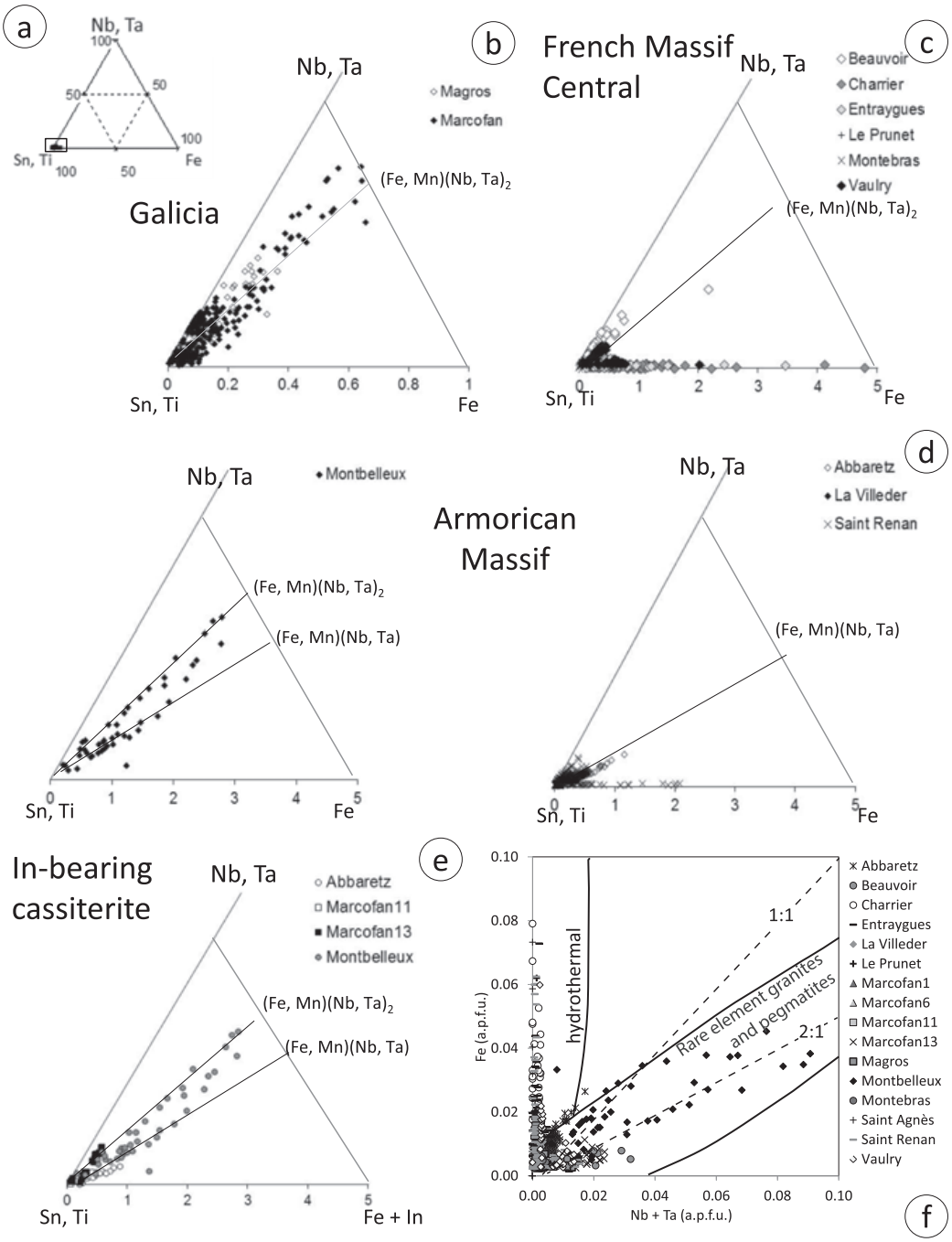

Fig. 4. (a) (Sn^{4+}, Ti^{4+})–(Nb^{5+}, Ta^{5+})–Fe ternary diagram showing chemical composition of all analysed cassiterite; (b) detail of this ternary diagram for cassiterite of Galicia (Spain); (c) detail of this ternary diagram for cassiterite of French Massif Central; (d) detail of this ternary diagram for cassiterite of French Armorican Massif; (e) detail of this ternary diagram for indium-bearing cassiterite of Abbaretz, Marcofán and Montbelleux; (f) binary diagram of (Nb + Ta) *vs*. (Fe + Mn) for cassiterite from all the studied deposits. The fields of hydrothermal cassiterite and cassiterite in rare element granites and pegmatites were defined by Tindle & Breaks (1998).

Abbaretz (schist-hosted), although the Sn mineralizations are considered to be associated with the same types of granite. In the La Chataigneraie district, hydrothermal Fe–Ti-rich and Nb–Ta-poor cassiterites disseminated in schists (Le Prunet, Entraygues) and Nb–Ta-rich magmatic cassiterite in the Entraygues leucogranite derived both from magmatic fluids (Lerouge *et al.*, 2007). These chemical variations of cassiterite from the different granite-related hydrothermal Sn mineralisations probably reflect the complex processes of Sn-ore deposition, including chemical heterogeneities of the peraluminous magmas (due to, *e.g.*, different degrees of partial melting, fractional crystallisation, different sediment sources), but also interactions of magma-derived fluids with various host-rocks (various compositions, *P–T* conditions) and mixing of magma-derived fluids with external fluids (meteoric, metamorphic) (Lehmann, 1990; Linnen & Cuney, 2005).

On this basis, the Fe *vs*. Nb+Ta diagram of Tindle & Breaks (1998) could be interesting to efficiently target hydrothermal Nb–Ta-rich cassiterites, which have a favourable chemistry for In incorporation in the cassiterite lattice.

6. Conclusion

The purpose of this work was to evaluate the distribution of In within Sn-polymetallic mineralizations in the western Variscan Belt, to discuss criteria favouring the presence of In within cassiterite, and to determine how In may be substituted. The EPMA analyses of cassiterite from the twelve Variscan Sn-polymetallic ore deposits and from the Ordovician Sn–W ore deposit of Montbelleux provide evidence of low substitution of Sn by Ti, Fe, Nb, Ta and In, highly dependent on ore type, magmatic processes, host rock, fluid/rock interaction processes, and fluid mixing. The highest Ti and Fe substitutions in cassiterite are observed in ores hosted by metapelitic schists. The highest Nb and Ta substitutions in cassiterite are observed in magmatic ores associated with rare-metal granites and in hydrothermal vein-type mineralizations genetically linked with peraluminous granites (Montbelleux, Marcofán and Abbaretz). The significant In content in hydrothermal cassiterites from Montbelleux, Marcofán and Abbaretz correlates with the highest levels of Nb, Ta and Fe substitution, allowing two coupled substitutions to be proposed: (1) 2 (Sn^{4+}, Ti^{4+}) ↔ (Fe^{3+}, In^{3+}) + (Nb^{5+}, Ta^{5+}) and (2) Fe^{2+} + (Nb, Ta)$^{5+}$ ↔ In^{3+} + (Ti, Sn)$^{4+}$, depending on the Fe valence. These substitutions may be limited by the co-formation of tantalite or other Ta-bearing minerals. Further micro-X-ray fluorescence spectrometry coupled with micro-X-ray diffraction and near-edge X-ray absorption fine structure (XANES) measurements at the Fe *K*-edge could be of major interest to further constrain substitution mechanisms and Fe valency, and the consequence of these substitutions on the cassiterite lattice. In all deposit types, sulfides are the dominant In carriers, notably stannite (up to 3000 ppm In), chalcopyrite (up to 2800 ppm In), pyrite (up to 1490 ppm In), sphalerite (up to 700 ppm In) and arsenopyrite (up to 740 ppm In). Interestingly, other oxides host In, notably rutile (up to 1100 ppm In).

Acknowledgements: Zdenek Johan was a high-level scientist in Mineralogy and Metallogeny, then Research Manager at BRGM for many years (1969–2000). He worked on geological processes associated to the formation of ore deposits, and specially on the metallogenesis of granite-related Sn and W. He published several papers on indium in sphalerite. The first author has had the privilege and the honour to work with him and his wife Věra. She will not forget their kindness and their passion to transmit and share their knowledge to others. This paper is dedicated to them.

This research has been financially supported by the BRGM Research. We would like to thank Michel Outrequin from Cameca (Genevilliers, France) for the FEG mapping. We are grateful to Dr Karen M. Tkaczyk (McMillan translation) for editing the English text. The Editor in Chief, Professor Reto Gieré, the Guest Associate Editor, Professor Vojtěch Ettler, Professor Thomas Seifert and two anonymous referees are thanked for their constructive comments, which contributed to improvement of the manuscript.

Uncited references

Q5

Cook et al. (2009) and Lerouge and Bouchot (2005).

References

Andersen, J.C.O., Stickland, R.J., Rollinson, G.K., Shail, R.K. (2016): Indium mineralisation in SW England: host parageneses and mineralogical relations. *Ore Geol. Rev.*, **78**, 213–238.

Bauer, M.E., Seifert, T., Krause, J., Burisch, M., Richter, N., Gutzmer, J. (2017): Indium-bearing sulphides from the Hämmerlein polymetallic skarn deposit, Germany – evidence for late stage diffusion of indium into sphalerite. *in* "Goldschmidt conference 2017, Paris, France", Goldschmidt Abstracts.

Benzaazoua, M., Marion, P., Pinto, A., Migeon, H., Wagner, F.E. (2003): Tin and indium mineralogy within selected samples from the Neves Corvo ore deposit (Portugal): a multidisciplinary study. *Miner. Eng.*, **16**, 1291–1302.

Bernard-Griffiths, J., Peucat, J.J., Sheppard, S., Vidal, P. (1985): Petrogenesis of Hercynian leucogranites from the southern Armorican Massif: contribution of REE and isotopic (Sr, Nd, Pb and O) geochemical data to the study of source rock characteristics and ages. *Earth Planet. Sci. Lett.*, **74**, 235–250.

Béziat, P. & Bornuat, M. (1995): Carte minière de la France métropolitaine à 1/1 000 000. Notice Explicative. Ministère de l'Industrie, BRGM, Service Minier National, 102 p.

Bouchot, V., Ledru, P., Lerouge, C., Lescuyer, J.-L., Milesi, J.-P. (2005): Late Variscan mineralizing systems related to orogenic processes: The French Massif Central. *Ore Geol. Rev.*, **27**, 169–197.

Boulandon, J. (1989): France and Luxembourg. *in* "Mineral Deposits of Europe", F.W. Dunning et al., eds. The Inst. Mining and Metallurgy, the Mineralogical Society, Oxford, v. 4/5, 37–104.

Breiter, K., Škoda, R., Uher, P. (2005): Nb–Ta–Ti–W–Sn-oxide minerals as indicators of a peraluminous P- and F-rich granitic system evolution: Podlesí, Czech Republic. *Mineral. Petrol.*, **91**, 225–248.

Briskey, J.A. (2005): Indium in lead–zinc and other mineral deposits. *in* USGS 2005. Open file report 2005-1209. URL: http://pubs.usgs.gov/of/2005/1209/2005-1209.pdf, 8p.

Cantinolle, P., Laforêt, C, Maurel, C., Picot, P., Grangeon, J. (1985): Contribution à la minéralogie de l'indium : Découverte en France de deux nouveaux sulfures d'indium et de deux nouvelles occurrences de roquésite. *Bull. Minéral.*, **108**, 245–248.

Černý, P., Blevin, P.L., Cuney, M., London, D. (2005): Granite-related ore deposits. Society of Economic Geologists, Inc., Economic Geology 100th Anniversary Volume, 337–370.

Černý, P., Roberts, W.L., Ercit, T.S., Chapman, R. (1985): Wodginite and associated minerals from the Peerless pegmatite, Pennington County, South Dakota. *Am. Mineral.*, **70**, 1044–1049.

Chauris, L. & Marcoux, E. (1994): Metallogeny of the Armorican Massif. *in* "Pre-Mesozoic geology in france and related areas", J.D. Keppie, ed. Springer-Verlag, Berlin, 243–264.

Chauris, L., Lulzac, Y., Cotten, J. (1989): Une lame de granite albitique tardi-cadomienne : le gisement stanno-wolframifère de Montbelleux (Massif Armoricain, France). *Chron. Rech. Min*., **496**, 25–39.

Cook, N.J., Ciobanu, C.L., Pring, A., Skinner, W., Shimizu, M., Danyushevsky, L., Saini-Eidukat, B., Melcher, F. (2009): Trace and minor elements in sphalerite: a LA-ICPMS study. *Geochim. Cosmochim. Acta*, **73**, 4761–4791.

Cook, N.J., Ciobanu, C.L., Williams, T. (2011a): The mineralogy and mineral chemistry of indium in sulphide deposits and implications for mineral processing. *Hydrometallurgy*, **108**, 226–228.

Cook, N.J., Ciobanu, C.L., Danyushevsky, L.V., Gilbert, S. (2011b): Minor and trace elements in bornite and associated Cu–(Fe)-sulfides: a LA-ICP-MS study of bornite mineral chemistry. *Geochim. Cosmochim. Acta*, **75**, 6473–6496.

Cook, N.J., Sundblad, K., Valkama, M., Nygård, R., Ciobanu, C.L., Danyushevsky, L. (2011c): Indium mineralisation in A-type granites in southeastern Finland: insights into mineralogy and partitioning between coexisting minerals. *Chem. Geol.*, **284**, 62–73.

Cuney, M., Marignac, C., Weisbrod, A. (1992): The Beauvoir topaz-lepidolite albite granite (Massif Central, France): the disseminated magmatic Sn–Li–Ta–Nb–Be mineralization. *Econ. Geol.* **87**, 1766–1794.

Dill, H.G., Garrido, M.M., Melcher, F., Gomez, M.C., Weber, B., Luna, L.I., Bahr, A. (2013): Sulfidic and non-sulfidic indium mineralization of the epithermal Au–Cu–Zn–Pb–Ag deposit San Roque (Provincia Rio Negro, SE Argentina) – with special reference to the "indium window" in zinc sulfide. *Ore Geol. Rev.*, **51**, 103–128.

EU Commission (2014): Report on critical raw materials for the EU. Report of the Ad-hoc Working Group on Defining Critical Raw Materials. http://ec.europa.eu/enterprise/policies/raw-materials/critical/index_en.htm (accessed on: 2015/03/01).

Faure, M., Sommers, C., Melleton, J., Cocherie, A., Lautout, O. (2008): The Léon Domain (French Massif Armoricain): a westward extension of the Mid-German Crystalline Rise? Structural and geochronological insights. *Int. J. Earth Sci.*, **99**, 65–81.

Faure, M., Lardeaux, J.M., Ledru, P. (2009): A review of the pre-Permian geology of the Variscan French Massif Central. *C. R. Geosci.*, **341**, 202–213.

Figueiredo, M.O., Pereira da Silva, T., de Oliveira, D., Rosa, D. (2012): Indium-carrier minerals in polymetallic sulphide ore deposits: a crystal chemical insight into an indium binding state supported by X-ray absorption spectroscopy data. *Minerals*, **2**, 426–434.

Fouillac, A.M. & Rossi, P. (1991): Near-solidus $\delta^{18}O$ depletion in a Ta–Nb-bearing albite granite – the Beauvoir granite, France. *Econ. Geol.*, **86**, 1704–1720.

Frenzel, M., Hirsch, T., Gutzmer, J. (2016): Corrigendum to "Gallium, germanium, indium and other trace and minor elements in sphalerite as a function of deposit type – a meta-analysis". *Ore Geol. Rev.,* **76**, 52–78.

George, L.L., Cook, N.J., Ciobanu, C.L. (2016): Partitioning of trace elements in co-crystallized sphalerite-galena-chalcopyrite hydrothermal ores. *Ore Geol. Rev.*, **77**, 97–116.

Gloaguen, E. (2006): Apports d'une étude intégrée sur les relations entre granites et minéralisations filoniennes (Au et Sn-W) en contexte tardiorogénique (Chaîne Hercynienne, Galice centrale, Espagne). PhD Thesis, Université d'Orléans, p. 572. http://tel.archives-ouvertes.fr/tel-00107391.

Gloaguen, E., Branquet, Y., Chauvet, A., Bouchot, V., Barbanson, L., Vigneresse, J.L. (2014): Tracing the magmatic/hydrothermal transition in regional low-strain zones: the role of magma dynamics in strain localization at pluton roof, implications for intrusion-related gold deposits. *J. Struct. Geol.*, **58**, 108–121.

Jeske, T. & Seifert, T. (2017): Late-Variscan Sn-polymetallic overprinting of the Pöhla-Hämmerlein skarn zone, Erzgebirge, Germany. *in* "Goldschmidt conference 2017, Paris, France", Goldschmidt Abstracts.

Jung, D. & Seifert, T. (1996): On the metallogeny of the late Hercynian tin deposit "Röhrenbohrer field"/Greifenstein area, Sn-W district Ehrenfriedersdorf-Geyer, Erzgebirge, Germany. *Freiberger Forschungshefte, TU Bergakademie Freiberg, C* **467**, 131–150.

Lehmann, B. (1990): Metallogeny of tin. Lecture Notes in Earth Sciences, Vol. 32. Springer-Verlag, Berlin, 211 p.

Lerouge, C. & Bouchot, V. (2005): Chataigneraie-example of a late Variscan tungsten district: Southern French Massif Central: Lat. 44°40′ N, Long. 2°35′ E. *Ore Geol. Rev.*, **27**, 200–201.

Lerouge, C., Bouchot, V., Guerrot, C. (2000): Fluids and the W–As ± Au ore deposits of the Enguialès-Leucamp District, La Châtaigneraie, French Massif Central. In Geofluids III Fluids in magmatic and metamorphic environments – Barcelona – Spain. *J. Geochem. Explor.*, **69–70**, 343–348.

Lerouge, C., Deschamps, Y., Piantone, P., Gilles, C., Breton, J. (2007): Metal-carrier accessory minerals associated with W ± Sn mineralization, La Châtaigneraie tungsten ore district, Massif Central, France. *Can. Mineral.*, **45**, 875–889.

Lescuyer, J.L., Leistel, J.M., Marcoux, E., Milési, J.P., Thiéblemont, D. (1998): Late Devonian-Early Carboniferous peak sulphide mineralization in the Western Hercynides. *Mineral. Dep.*, **33**, 208–220.

Linnen, R.L. & Cuney, M. (2005): Granite-related rare-element deposits and experimental constraints on Ta–Nb–W–Sn–Zr–Hf mineralization. *in* "Rare-Element Geochemistry and Mineral Deposits", R.L. Linnen & I.M. Samson, eds. *Geological Association of Canada, GAC, Short Courses Notes*, **17**, 45–68.

Maierová, P., Schulmann, K., Lexa, O., Guillot, S., Štípská, P., Janoušek, V., Čadek, O. (2016): European Variscan orogenic evolution as an analogue of Tibetan-Himalayan orogen: insights from petrology and numerical modeling. *Tectonics*, **35**, 2015TC004098, doi:10.1002/2015TC004098.

Marignac, C. & Cuney, M. (1999): Ore deposits of the French Massif Central: insight into the metallogenesis of the Variscan collision belt. *Mineral. Depos.*, **34**, 472–504.

Melleton, J., Cocherie, A., Faure, M., Rossi, P. (2010): Precambrian protoliths and Early Paleozoic magmatism in the French Massif Central: U–Pb data and the North Gondwana connection in the west European Variscan belt. *Gondwana Res.*, **17**, 13–25.

Melleton, J., Gloaguen, E., Frei, D. (2015): Rare-elements (Li–Be–Ta–Sn–Nb) magmatism in the European Variscan belt, a review. *in* "Proceedings 13th SGA biennial meeting, 24–27 August, 2015, Nancy, France", vol. 2, 807–810.

Möller, P., Dulski, P., Szacki, W., Malow, G., Riedel, E. (1988): Substitution of tin in cassiterite by tantalum, niobium, tungsten, iron and manganese. *Geochim. Cosmochim. Acta*, **52**, 1497–1503.

Neiva, A.M.R. (2008): Geochemistry of cassiterite and wolframite from tin and tungsten quartz veins in Portugal. *Ore Geol. Rev.*, **33**, 221–238.

Pavlova, G.G., Palessky, S.V., Borisenko, A.S., Vladimirov, A.G., Seifert, T., Phan, L.A. (2015) Indium in cassiterite and ores of tin deposits. *Ore Geol. Rev.*, **66**, 99–113.

Picot, P. & Pierrot, R. (1963): Mine de Charrier. *Bull. Soc. fr. Minéral. Cristallogr.*, **86**, 7–14.

Pinto, A., Relvas, J.M.R.S., Carvalho, J.R.S., Liu Y., Pacheco, N., Pinto, F., Fonseca, R. (2014): High-tech metals in the zinc-rich massive ores of the Neves Corvo Deposit. *Comunicações Geológicas 101, Especial II*, 825–828.

Pouchou, J.L. & Pichoir, F. (1984): A new model for quantitative microanalysis – Part 1: application to the analysis of homogeneous samples. *Rech. Aerosp.*, **3**, 13–38.

Raimbault, L., Cuney, M., Azencott, C., Duthou, J.L., Joron, J.L. (1995): Geochemical evidence for a multistage magmatic genesis of Ta–Sn–Li mineralization in the granite at Beauvoir, French Massif Central. *Econ. Geol.*, **90**, 548–576.

Schuppan, W. & Hiller, A. (2012): Die Komplexlagerstätten Tellerhäuser und Hämmerlein. Bergbau in Sachsen, Band 17 Bergbaumonografie, Freiberg, 162 p.

Schwarz-Schampera, U. (2014): Indium. *in* "Critical metals handbook", G. Gun, ed. John Wiley & Sons, 204–229.

Schwartz-Schampera, U. & Herzig, P.M. (2002): Indium: geology. Mineralogy and economics. *in* "Geosciences". Springer-Verlag, Heidelberg, Germany, vol. XII, 257 p.

Seifert, T. (2008): Metallogeny and petrogenesis of lamprophyres in the mid-European variscides – post-collisional magmatism and its relationship to late-variscan ore forming processes (Bohemian Massif). IOS Press BV, Amsterdam, Netherlands, 303 p.

— (2015): Paragenesis, geochemistry and age of late-Variscan Sn, In and Ag mineralization in the Marienberg district and its relationship to mafic and acidic magmatic events, Erzgebirge, Germany. *in* "13th SGA Biennial Meeting, 24–27 August, 2015, Nancy, France", Ext Abstract, 843–846.

Seifert, T. & Sandmann, D. (2006): Mineralogy and geochemistry of indium-bearing polymetallic vein-type deposits: implications for host minerals from the Freiberg district, Eastern Erzgebirge, Germany. *Ore Geol. Rev.,* **28**: 1–31.

Seifert, T., Baumann, L., Jung, D. (1992): On the Problem of the relationship between Sn(-W) and Quartz-Polymetal Mineralizations in the Marienberg Deposit District. *Z. Geol. Wiss.*, **20**, 371–392.

Seifert, T., Chaplygin, I.V., Yudovskaya, M.A., Chaplygin, O. (2015): Mantle-derived In mineralization in the Erzgebirge and Kuril Island Arc. *in* "Goldschmidt Conference 2015, Prague, Czech Republic", Goldschmidt Abstracts, 2835.

Shimizu, M., Furuhashi, T., Harada, A., Cook, N.J. (2008): Indium mineralization in epithermal Au–Ag–Cu–Mn–Te–Se–Bi–Sn–Mo vein-type deposits of the Kawazu (Rendaiji) mine, Shizuoka Prefecture, Japan. *in* "33rd Int. Geol. Congr., Oslo, 6–14 August, 2008", Abstract CD-ROM.

Simons, B., Shail, R.K., Andersen, J.C.O. (2016): The petrogenesis of the Early Permian Variscan granites of the Cornubian Batholith: lower plate post-collisional peraluminous magmatism in the Rhenohercynian Zone of SW England. *Lithos*, **260**, 76–94.

Sizaret, S., Branquet, Y., Gloaguen, E., Chauvet, A., Barbanson, L., Arbaret, L., Chen, Y. (2009): Estimating the local paleo-fluid flow velocity: new textural method and application to metasomatism. *Earth Planet. Sci. Lett.,* **280**, 71–82.

Smith, I.C., Carson, B.L., Hoffmeister, F. (1978): Trace metals in the environment, Volume 5 – Indium. Ann Arbor Science Publishers Inc., Ann Arbor, 1978, 552 p.

Tartèse, R. & Boulvais, P. (2010): Differentiation of peraluminous leucogranites "en route" to the surface. *Lithos*, **114**, 353–368.

Tindle, A.G. & Breaks, F.W. (1998): Oxide minerals of the Separation Rapids rare-element granitic pegmatite group, northwestern Ontario. *Can. Mineral.*, **36**, 609–635.

Valkama, M., Sundblad, K., Nygård, R., Cook, N. (2016): Mineralogy and geochemistry of indium-bearing polymetallic veins in the Sarvlaxviken area, Lovisa, Finland. *Ore Geol. Rev.*, **75**, 206–219.

Vallance, J., Cathelineau, M., Marignac, C., Boiron, M.C., Fourcade, S., Martineau, F., Fabre, C. (2001): Microfracturing and fluid mixing in granites; W-(Sn) ore deposition at Vaulry (NW French Massif Central). *Tectonophysics*, **336**, 43–61.

Werner, T.T., Mudd, G.M., Jowitt, S.M. (2017): The world's by-product and critical metal resources part III: a global assessment of indium. *Ore Geol. Rev.*, in press.

Williamson, B.J., Shaw, A., Downes, H., Thirlwall, M.F. (1996): Geochemical constraints on the genesis of Hercynian two-mica leucogranites from the Massif Central, France. *Chem. Geol.*, **127**, 1–25–42.

Zhang, K., Wu, Y., Wang, W., Li, B., Zhang, Y., Zuo, T. (2015): Recycling indium from waste LCDs: A review. *Resour. Conserv. Recycl.*, **104**, 276–290.

Received 1 December 2016
Modified version received 1 June 2017
Accepted 2 June 2017